

Magnetic data radial inversion for 3-D source geometry estimation

L.B. Vital^{1*}

¹ *Observatório Nacional, Gal. José Cristino, 77, São Cristóvão, Rio de Janeiro, 20921-400, Brazil*

Key words: Numerical solutions; Inverse theory; Magnetic anomalies.

* Observatório Ncional, ON

1 METHODOLOGY

1.1 Forward problem

Let \mathbf{d}^o be the observed data vector, whose i th element d_i^o , $i = 1, \dots, N$, is the total-field anomaly produced by a 3-D source (Fig. 1a) at the point (x_i, y_i, z_i) of a Cartesian coordinate system with x , y and z axes pointing to north, east and down, respectively. We assume that the direction of the total magnetization vector of the source is constant and known. We approximate the volume of the source by a set of L vertically juxtaposed 3-D prisms (Fig. 1b) by following the same approach of Oliveira Jr. et al. (2011) and Oliveira Jr. & Barbosa (2013). The depth to the top of the shallowest prism is defined by z_0 and m_0 is the constant total-magnetization intensity of all prisms. The horizontal cross-section of each prism is described by a polygon with a fixed number V of vertices equally spaced from 0° to 360° , which are described in polar coordinates referred to an internal origin O^k . The radii of the vertices $(r_j^k, j = 1, \dots, V, k = 1, \dots, L)$, the horizontal coordinates $(x_0^k$ and $y_0^k, k = 1, \dots, L)$ of the origins $O^k, k = 1, \dots, L$, and the depth extent dz of the L vertically stacked prisms (Fig. 1b) are arranged in a $M \times 1$ parameter vector \mathbf{p} , $M = L(V + 2) + 1$, given by

$$\mathbf{p} = \begin{bmatrix} \mathbf{r}^{1\top} & x_0^1 & y_0^1 & \dots & \mathbf{r}^{L\top} & x_0^L & y_0^L & dz \end{bmatrix}^\top, \quad (1)$$

where “ \top ” denotes transposition and \mathbf{r}^k is a $V \times 1$ vector containing the radii r_j^k of the k th prism. Let $\mathbf{d}(\mathbf{p})$ be the predicted data vector, whose i th element

$$d_i(\mathbf{p}) \equiv \sum_{k=1}^L f_i^k(\mathbf{r}^k, x_0^k, y_0^k, dz, z_1^k, m_0), \quad i = 1, \dots, N, \quad (2)$$

is the total-field anomaly produced by the ensemble of L prisms at the i th observation point (x_i, y_i, z_i) . In eq. 2, $f_i^k(\mathbf{r}^k, x_0^k, y_0^k, dz, z_1^k, m_0)$ is the total-field anomaly produced, at the observation point (x_i, y_i, z_i) , by the k th prism, with depth to the top $z_1^k = z_0 + (k - 1)dz$. We calculate $d_i(\mathbf{p})$ (eq. 2) by using the Python package Fatiando a Terra (Uieda et al. 2013), which implements the formulas proposed by Plouff (1976).

1.2 Inverse problem formulation

Given a set of tentative values for depth to the top of the shallowest prism z_0 and for the intensity of the total-magnetization of the source m_0 , we solve a constrained non-linear problem to estimate the parameter vector \mathbf{p} (eq. 1) by minimizing the goal function

$$\Gamma(\mathbf{p}) = \phi(\mathbf{p}) + \sum_{\ell=1}^7 \alpha_\ell \varphi_\ell(\mathbf{p}), \quad (3)$$

subject to

$$p_l^{min} < p_l < p_l^{max}, \quad l = 1, \dots, M, \quad (4)$$

where $\varphi(\mathbf{p})$ is the data-misfit function given by

$$\phi(\mathbf{p}) = \frac{1}{N} \|\mathbf{d}^o - \mathbf{d}(\mathbf{p})\|_2^2, \quad (5)$$

which represents the normalized squared Euclidean norm of the difference between the observed data vector \mathbf{d}^o and the predicted data vector $\mathbf{d}(\mathbf{p})$, α_ℓ is a positive number representing the weight of the ℓ th constraint function $\varphi_\ell(\mathbf{p})$ and p_l^{min} and p_l^{max} are, respectively, the lower and upper limits for the l th element p_l of the parameter vector \mathbf{p} (eq. 1). These limits are defined by the interpreter based on both the horizontal extent of the magnetic anomaly and the knowledge about the source. Details about the regularizing functions $\varphi_\ell(\mathbf{p})$, $\ell = 1, \dots, 7$, and the numerical procedure to solve this nonlinear inverse problem are given in the following sections.

1.3 Constraint functions

We have divided the constraint functions $\varphi_\ell(\mathbf{p})$ (eq. 3), $\ell = 1, \dots, 7$, used here to obtain stable solutions and introduce a priori information about the magnetic source into three groups.

1.3.1 Smoothness constraints

This group is formed by variations of the first-order Tikhonov regularization (Aster et al. 2019, p. 103) and impose smoothness on the radii r_j^k and the Cartesian coordinates x_0^k and y_0^k of the origin O^k , $j = 1, \dots, V$, $k = 1, \dots, L$, defining the horizontal section of each prism (Fig. 1b). They were proposed by Oliveira Jr. et al. (2011) and Oliveira Jr. & Barbosa (2013) and play a very role in introducing a prior information about the shape of the source.

The first constraint of this group is the *Smoothness constraint on the adjacent radii defining the horizontal section of each vertical prism*. This constraint imposes that adjacent radii r_j^k and r_{j+1}^k within each prism must be close to each other. It forces the estimated prism to be approximately cylindrical. Mathematically, the constraint is given by

$$\varphi_1(\mathbf{p}) = \sum_{k=1}^L \left[(r_V^k - r_1^k)^2 + \sum_{j=1}^{V-1} (r_j^k - r_{j+1}^k)^2 \right]. \quad (6)$$

We have conveniently rewritten this constraint in matrix form as follows:

$$\varphi_1(\mathbf{p}) = \mathbf{p}^\top \mathbf{R}_1^\top \mathbf{R}_1 \mathbf{p}, \quad (7)$$

where

$$\mathbf{R}_1 = \begin{bmatrix} \mathbf{S}_1 & \mathbf{0}_{LV \times 1} \end{bmatrix}_{LV \times M}, \quad (8)$$

$$\mathbf{S}_1 = \mathbf{I}_L \otimes \begin{bmatrix} (\mathbf{I}_V - \mathbf{D}_V^\top) & \mathbf{0}_{V \times 2} \end{bmatrix}, \quad (9)$$

$\mathbf{0}_{LV \times 1}$ is an $LV \times 1$ vector with null elements, \mathbf{I}_L is the identity matrix of order L , “ \otimes ” denotes the Kronecker product (Horn & Johnson 1991, p. 243), $\mathbf{0}_{V \times 2}$ is a $V \times 2$ matrix with null elements, \mathbf{I}_V is the identity matrix of order V and \mathbf{D}_V^\top is the upshift permutation matrix of order V (Golub & Loan 2013, p. 20).

The second constraint of this group is the *Smoothness constraint on the adjacent radii of the vertically adjacent prisms*, which imposes that adjacent radii r_j^k and r_j^{k+1} within vertically adjacent prisms must be close to each other. This constraint forces the shape of all prisms to be similar to each other and is given by

$$\varphi_2(\mathbf{p}) = \sum_{k=1}^{L-1} \left[\sum_{j=1}^V (r_j^{k+1} - r_j^k)^2 \right], \quad (10)$$

in matrix form:

$$\varphi_2(\mathbf{p}) = \mathbf{p}^\top \mathbf{R}_2^\top \mathbf{R}_2 \mathbf{p}, \quad (11)$$

where

$$\mathbf{R}_2 = \begin{bmatrix} \mathbf{S}_2 & \mathbf{0}_{(L-1)V \times 1} \end{bmatrix}_{(L-1)V \times M}, \quad (12)$$

$$\mathbf{S}_2 = \left(\begin{bmatrix} \mathbf{I}_{L-1} & \mathbf{0}_{(L-1) \times 1} \end{bmatrix} - \begin{bmatrix} \mathbf{0}_{(L-1) \times 1} & \mathbf{I}_{L-1} \end{bmatrix} \right) \otimes \begin{bmatrix} \mathbf{I}_V & \mathbf{0}_{V \times 2} \end{bmatrix}, \quad (13)$$

$\mathbf{0}_{(L-1)V \times 1}$ is an $(L-1)V \times 1$ vector with null elements, $\mathbf{0}_{(L-1) \times 1}$ is an $(L-1) \times 1$ vector with null elements and \mathbf{I}_{L-1} is the identity matrix of order $L-1$.

The last constraint of this group is the *Smoothness constraint on the horizontal position of the arbitrary origins of the vertically adjacent prisms*. This constraint imposes that the estimated horizontal Cartesian coordinates (x_0^k, y_0^k) and (x_0^{k+1}, y_0^{k+1}) of the origins O^k and O^{k+1} of adjacent prisms must be close to each other. It forces the prisms to be vertically aligned. This constraint is given by

$$\varphi_3(\mathbf{p}) = \sum_{k=1}^{L-1} \left[(x_0^{k+1} - x_0^k)^2 + (y_0^{k+1} - y_0^k)^2 \right], \quad (14)$$

in matrix form:

$$\varphi_3(\mathbf{p}) = \mathbf{p}^\top \mathbf{R}_3^\top \mathbf{R}_3 \mathbf{p}, \quad (15)$$

where

$$\mathbf{R}_3 = \begin{bmatrix} \mathbf{S}_3 & \mathbf{0}_{(L-1)2 \times 1} \end{bmatrix}_{(L-1)2 \times M}, \quad (16)$$

$$\mathbf{S}_3 = \left(\begin{bmatrix} \mathbf{I}_{L-1} & \mathbf{0}_{(L-1) \times 1} \end{bmatrix} - \begin{bmatrix} \mathbf{0}_{(L-1) \times 1} & \mathbf{I}_{L-1} \end{bmatrix} \right) \otimes \begin{bmatrix} \mathbf{0}_{2 \times V} & \mathbf{I}_2 \end{bmatrix}, \quad (17)$$

$\mathbf{0}_{(L-1)2 \times 1}$ is an $(L-1)2 \times 1$ vector with null elements, $\mathbf{0}_{2 \times V}$ is a $2 \times V$ matrix with null elements and \mathbf{I}_2 is the identity matrix of order 2.

1.3.2 Equality constraints

This group if formed by two constraints that were proposed by Oliveira Jr. et al. (2011) and Oliveira Jr. & Barbosa (2013) by following the same approach proposed Barbosa et al. (1997) and ?. They introduce a priori information about the shallowest prism and are suitable for outcropping sources.

The *Source's outcrop constraint* imposes that the horizontal cross-section of the shallowest prism must be close to the intersection of the geologic source with the known outcropping boundary. The matrix form of the this constraint is given by

$$\varphi_4(\mathbf{p}) = \left[(x_0^1 - x_0^0)^2 + (y_0^1 - y_0^0)^2 + \sum_{j=1}^V (r_j^1 - r_j^0)^2 \right], \quad (18)$$

in matrix form:

$$\varphi_4(\mathbf{p}) = (\mathbf{R}_4\mathbf{p} - \mathbf{a})^\top (\mathbf{R}_4\mathbf{p} - \mathbf{a}), \quad (19)$$

where \mathbf{a} is a vector containing the radii and the horizontal Cartesian coordinates of the polygon defining the outcropping boundary

$$\mathbf{a} = \begin{bmatrix} \tilde{r}_1^0 & \dots & \tilde{r}_V^0 & \tilde{x}_0^0 & \tilde{y}_0^0 \end{bmatrix}^\top, \quad (20)$$

and

$$\mathbf{R}_4 = \left[\mathbf{I}_{V+2} \quad \mathbf{0}_{(V+2) \times (M-V-2)} \right]_{(V+2) \times M}, \quad (21)$$

where \mathbf{I}_{V+2} is the identity matrix of order $V+2$ and $\mathbf{0}_{(V+2) \times (M-V-2)}$ is a matrix with null elements.

The *Source's horizontal location constraint* imposes that the horizontal Cartesian coordinates of the origin within the shallowest prism must be as close as possible to a known outcropping point. The matrix form of the this constraint is given by

$$\varphi_5(\mathbf{p}) = \left[(x_0^1 - x_0^0)^2 + (y_0^1 - y_0^0)^2 \right], \quad (22)$$

in matrix form:

$$\varphi_5(\mathbf{p}) = (\mathbf{R}_5\mathbf{p} - \mathbf{b})^\top (\mathbf{R}_5\mathbf{p} - \mathbf{b}), \quad (23)$$

where \mathbf{b} is a vector containing the horizontal Cartesian coordinates of the outcropping point

$$\mathbf{b} = \begin{bmatrix} \tilde{x}_0^0 & \tilde{y}_0^0 \end{bmatrix}^\top, \quad (24)$$

and

$$\mathbf{R}_5 = \begin{bmatrix} \mathbf{0}_{2 \times V} & \mathbf{I}_2 & \mathbf{0}_{2 \times (M-V-2)} \end{bmatrix}_{2 \times M}, \quad (25)$$

where \mathbf{I}_2 is the identity matrix of order 2 and $\mathbf{0}_{2 \times (M-V-2)}$ and $\mathbf{0}_{2 \times V}$ are matrices with null elements.

1.3.3 Minimum Euclidean norm constraints

Two constraints use the zeroth-order Tikhonov regularization with the purpose of obtaining stable solutions without necessarily introducing significant a priori information about the source.

The *Minimum Euclidean norm of the radii* imposes that all estimated radii within each prism must be close to null values. This constraint were proposed by Oliveira Jr. et al. (2011) and Oliveira Jr. & Barbosa (2013) and can be rewritten in matrix form as follows

$$\varphi_6(\mathbf{p}) = \sum_{k=1}^L \sum_{j=1}^V \left(r_j^k \right)^2. \quad (26)$$

in matrix form:

$$\varphi_6(\mathbf{p}) = \mathbf{p}^\top \mathbf{R}_6^\top \mathbf{R}_6 \mathbf{p}, \quad (27)$$

where

$$\mathbf{R}_6 = \begin{bmatrix} \mathbf{S}_6 & \mathbf{0}_{(M-1) \times 1} \\ \mathbf{0}_{1 \times (M-1)} & 0 \end{bmatrix}_{M \times M}, \quad (28)$$

and

$$\mathbf{S}_6 = \begin{bmatrix} \mathbf{I}_V & \mathbf{0}_{V \times 2} \\ \mathbf{0}_{2 \times V} & \mathbf{I}_2 \end{bmatrix}_{(V+2) \times (V+2)}. \quad (29)$$

The other constraint, the *Minimum Euclidean norm of the thickness*, imposes that the thickness of all prisms must be close to zero. This constraint were developed here to introduce a priori information about the maximum depth of the source. Its matrix form is given by

$$\varphi_7 = dz^2, \quad (30)$$

in matrix form:

$$\varphi_7 = \mathbf{p}^\top \mathbf{R}_7^\top \mathbf{R}_7 \mathbf{p}, \quad (31)$$

where

$$\mathbf{R}_7 = \begin{bmatrix} \mathbf{0}_{(M-1) \times (M-1)} & \mathbf{0}_{(M-1) \times 1} \\ \mathbf{0}_{1 \times (M-1)} & 1 \end{bmatrix}_{M \times M}. \quad (32)$$

1.4 Computational procedures

To estimate the parameter vector \mathbf{p} (eq. 1) that minimizes the goal function $\Gamma(\mathbf{p})$ (eq. 3), subjected to the inequality constraint (eq. 4), we use the Levenberg-Marquardt method (Aster et al. 2019, p. 240), and the inequality constraint (eq. 4) is incorporated using the same strategy used by Barbosa et al. (1999b). All derivatives of the misfit function $\phi(\mathbf{p})$ (eq. 5) with respect to the parameters are computed using a finite-difference approximation.

1.4.1 Considerations about the weights $\alpha_1, \alpha_2, \alpha_3, \alpha_4, \alpha_5, \alpha_6$, and α_7

Attributing the values to the weights α_ℓ (eq. 3) consists in an important feature of our method. However, there is no analytical rule to define them, so their values can be dependent on the particular characteristics of the interpretation model. To overcome this problem, we normalize the α_ℓ values as follows:

$$\alpha_\ell = \tilde{\alpha}_\ell \frac{E_\phi}{E_\ell}, \quad \ell = 1, \dots, 7, \quad (33)$$

where $\tilde{\alpha}_\ell$ is a positive scalar and E_ϕ/E_ℓ is a normalizing constant. In this equation, E_ℓ represents the median of the elements forming the main diagonal of the Hessian matrix of the ℓ th constraining function $\varphi_\ell(\mathbf{p})$ (eqs 6, 10, 14, 18, 22, 26, and 30). The constant E_ϕ is defined in a similar way using the Hessian matrix of the misfit function $\phi(\mathbf{p})$ (eq. 5) computed with the initial approximation \mathbf{p}_0 for the parameter vector \mathbf{p} (eq. 1) at the inversion algorithm. According to this empirical strategy, the weights α_ℓ are defined using the positive scalars $\tilde{\alpha}_\ell$ (eq. 33), which are less dependent on the particular characteristics of the interpretation model.

1.4.2 Inversion algorithm

At first, the inequality constraint (eq. 4) is incorporated on the parameter vector \mathbf{p} element by element obtaining the transformed parameter vector $\mathbf{p}^\dagger = f(\mathbf{p})$ as follows

$$p_l^\dagger = f(p_l) = -\ln \left(\frac{p_l^{\max} - p_l}{p_l - p_l^{\min}} \right), \quad (34)$$

where p_l , p_l^{\max} , and p_l^{\min} are the l th elements of \mathbf{p} , \mathbf{p}^{\max} and \mathbf{p}^{\min} , respectively. This equation is a homeomorphic transformation that has the inverse transformation given by

$$p_l = p_l^{\min} + \left(\frac{p_l^{\max} - p_l^{\min}}{1 + e^{-p_l^\dagger}} \right). \quad (35)$$

The estimated correction $\Delta\hat{\mathbf{p}}_k$ (where “~” denotes estimated) for the parameter vector \mathbf{p}_k for the nonlinear inverse problem at the k th iteration is obtained by solving the linear system given by

$$\mathbf{D}_k \left[\mathbf{D}_k \mathbf{H}^\dagger(\hat{\mathbf{p}}_k) \mathbf{D}_k + \lambda_k \mathbf{I} \right] \mathbf{D}_k \Delta\hat{\mathbf{p}}_k^\dagger = -\nabla\Gamma(\hat{\mathbf{p}}), \quad (36)$$

λ_k is a positive scalar to regularize the steps of the inversion ensuring the convergence of the algorithm which varies at each iteration by a scalar $d\lambda$ described in the algorithm, \mathbf{I} is a identity matrix with dimension $M \times M$, and $\nabla\Gamma(\hat{\mathbf{p}})$ is the gradient of the goal function (eq. 3) plus the gradient of each constraint function (eqss 6, 10, 14, 18, 22, 26, and 30). In this equation, $\mathbf{H}^\dagger(\mathbf{p}_k^\dagger)$ is given by

$$\mathbf{H}^\dagger(\mathbf{p}_k) = \mathbf{H}(\mathbf{p}_k)\mathbf{T}(\mathbf{p}_k), \quad (37)$$

where $\mathbf{H}(\mathbf{p}_k)$ is the Hessian matrix of $\Gamma(\mathbf{p})$ plus the Hessian matrix of each constraint function (eqss 6, 10, 14, 18, 22, 26, and 30) and $\mathbf{T}(\mathbf{p}_k)$ is a diagonal matrix that incorporates the inequality constraint on $\mathbf{H}^\dagger(\mathbf{p}_k)$ which the l th non-zero element given by

$$\mathbf{T}_{ll} = \frac{(p_l^{max} - p_l)(p_l - p_l^{min})}{p_l^{max} - p_l^{min}}, \quad l = 1, \dots, M. \quad (38)$$

Marquardt (1963) suggests a normalization on $\mathbf{H}^\dagger(\mathbf{p}_k)$ to balance the magnitude of λ_k and the diagonal of $\mathbf{H}^\dagger(\mathbf{p}_k)$. To introduce this normalization, we use the diagonal matrix \mathbf{D}_k whose l th non-zero element d_{ll} given by

$$d_{ll} = \frac{1}{\sqrt{h_{ll}^\dagger}}, \quad (39)$$

where h_{ll}^\dagger is the l th element of the diagonal of $\mathbf{H}^\dagger(\mathbf{p}_k)$. The effect of this normalization is introduced and removed in the equation 36.

The proposed methodology was implemented using the following algorithm:

- (i) Iteration $k = 0$: input z_0 , m_0 , \mathbf{d}^o , \mathbf{p}^{min} , \mathbf{p}^{max} , $\tilde{\alpha}_1, \tilde{\alpha}_2, \tilde{\alpha}_3, \tilde{\alpha}_4, \tilde{\alpha}_5, \tilde{\alpha}_6, \tilde{\alpha}_7$, and an initial approximation \mathbf{p}_0 satisfying the inequality constraints (eq. 4);
- (ii) obtain \mathbf{H}_0 and $\alpha_1, \alpha_2, \alpha_3, \alpha_4, \alpha_5, \alpha_6$, and α_7 (eq. 33);
- (iii) obtain \mathbf{p}_k^\dagger and $\mathbf{H}^\dagger(\mathbf{p}_k)$ using equations 34 and 37, respectively;
- (iv) obtain $\Delta\hat{\mathbf{p}}_k^\dagger$ at the k th iteration by solving equation 36;
- (v) compute: $\hat{\mathbf{p}}_{k+1}^\dagger = \hat{\mathbf{p}}_k^\dagger + \Delta\hat{\mathbf{p}}_k^\dagger$;
- (vi) obtain $\hat{\mathbf{p}}_{k+1}$ using the inverse inequality function (eq. 35);
- (vii) Test for algorithm convergence. Evaluate $|\Gamma(\hat{\mathbf{p}}_{k+1}) - \Gamma(\hat{\mathbf{p}}_k)|$.

where $\Gamma(\mathbf{p}^{k+1})$ and $\Gamma(\mathbf{p}^k)$ are the goal function (eq. 3) evaluated at the iteration $k + 1$ and k , respectively.

1.4.3 Practical considerations

Our algorithm depends on several parameters that significantly impact the estimated models and cannot be automatically set without the interpreter's judgment. They are the parameters $\tilde{\alpha}_1, \tilde{\alpha}_2, \tilde{\alpha}_3, \tilde{\alpha}_4$,

$\tilde{\alpha}_5$, $\tilde{\alpha}_6$, and $\tilde{\alpha}_7$. Based on our practical experience, we suggest some empirical procedures for setting these parameters.

The parameters $\tilde{\alpha}_1$ and $\tilde{\alpha}_2$ impose priori information on the shape of the horizontal cross-section of the prisms. Generally, they have values close to each other varying from 10^{-5} to 10^{-4} . If $\tilde{\alpha}_1 > \tilde{\alpha}_2$ the prisms will have a very smooth horizontal cross-section, close to a circular shape. On the other hand, if $\tilde{\alpha}_1 < \tilde{\alpha}_2$, than the difference on the shape of the horizontal cross-sections of the estimated model between vertically adjacent prisms will be smooth.

To control the alignment of the estimated model, the parameter $\tilde{\alpha}_3$ should be in a range from 10^{-5} to 10^{-3} . This parameter allows or forbids the estimated model to dip. Empirically, the value for this parameter follows the value for $\tilde{\alpha}_1$ and $\tilde{\alpha}_2$, they are usually close.

The parameter $\tilde{\alpha}_6$ imposes mathematical priori information on the inverse problem to control the convergence of the algorithm. We suggest that the value for this parameter should be two or three orders of magnitude greater than $\tilde{\alpha}_1$ and $\tilde{\alpha}_2$.

To control the depth extent of the estimated model, the parameter $\tilde{\alpha}_7$ should be in a range from 10^{-6} to 10^{-4} . This parameter depends on the depth extent of the initial approximate, it can decrease the depth extent or keep it close to the initial one. Normally, we suggest $\tilde{\alpha}_7 = 10^{-5}$ for a initial value.

An important aspect of our method is the choice of the initial approximation. For simplicity, we use a cylinder shape as an initial approximation located the initial cylinder on the center of the anomaly. We suggest that the cylinder radius should involves a great part, both positive and negative, of the horizontal size of the anomaly. Also, the depth extent dz of the cylinder should be greater than the true source. We suggest that the data produced by the initial approximation fit qualitatively the observations.

2 APPLICATION TO SYNTHETIC DATA

2.1 Simple model test

We have simulated a funnel-shaped source with simple geometry (blue prisms in Figs 3b and 5), which extends from $z_0 = 0$ m to 1600 m along depth and satisfies most of the constraints described in subsection 1.3. It is formed by $L = 8$ prisms, all of them with the same number of vertices $V = 20$, depth extent $dz = 200$ m and horizontal coordinates $(x_0^k, y_0^k) = (0, 0)$ m of the origins O^k , $k = 1, \dots, L$. The radii of all vertices are equal to each other within the same prism and decrease linearly with depth, varying from $r_j^0 = 1920$ m, at the shallowest prism, $r_j^L = 800$ m, at the deepest prism, $j = 1, \dots, V$. All prisms have the same total-magnetization direction with inclination -21.5° , declination -18.7° and intensity $m_0 = 9$ A/m. We calculated the total-field anomaly produced by this simple source on an 100 km^2 area, simulating an airborne survey composed of 20 flight lines that are equally spaced 500 m apart along the y axis, at a constant vertical coordinate $z = -150$ m. At each line, the data are spaced XX m apart along x axis. The total-field anomaly is corrupted with a pseudo-random Gaussian noise having mean and standard deviation equal to 0 nT and 5 nT, respectively (Fig. 3a).

We have inverted the synthetic total-field anomaly (Fig. 3a) produced by the simple source and obtained 36 different models. Each model was obtained by using a different pair of depth to the top z_0 and total-magnetization intensity m_0 (Fig. 4). All models were generated by using the true values of total-magnetization inclination and declination, the same interpretation model formed by $L = 5$ prisms, each one with $V = 20$ vertices, and the same weights for the constraining functions: $\tilde{\alpha}_1 = 10^{-4}$, $\tilde{\alpha}_2 = 10^{-4}$, $\tilde{\alpha}_3 = 10^{-4}$, $\tilde{\alpha}_4 = 0$, $\tilde{\alpha}_5 = 0$, $\tilde{\alpha}_6 = 10^{-6}$, and $\tilde{\alpha}_7 = 10^{-4}$. The initial approximation for all models have the same constant radii $r_j^k = 2000$ m, $k = 1, \dots, L$, $j = 1, \dots, V$, the same depth extent $dz = 350$ m and the same origin $(x_0^k, y_0^k) = (0, 0)$ m for all prisms.

Fig. 4 shows that the estimated model obtained by using the true values for depth to the top z_0 and total-magnetization intensity m_0 (represented by the red triangle in Fig. 4) produces the lowest value of goal function $\Gamma(p)$ (eq. 3). Fig. 5 shows that this estimated model (red prisms in Figs 5c and d) not only fits the noise-corrupted data, but also retrieves the geometry of the true source (blue prisms). The estimated depth extent of each prism is $dz = 297.65$ m, which results in a total depth extent (1485 m) very close to the true one (1600 m). These results illustrate the good performance of our method in an ideal case.

2.2 Complex model test

The second synthetic source has $L = 10$ prisms, each one with $M = 30$ vertices, and a total magnetization with $m_0 = 12$ A/m. The complex model has both induced and remnant magnetization with inclination -50° , and declination 9° . Its depth to the top is at $z_0 = 200$ m and its bottom is at 5700 m. The radii of the vertices ($r_j^k, j = 1, \dots, M, k = 1, \dots, L$) forming this synthetic body vary from 240 to 1540 m and the horizontal coordinates x_0 and y_0 of the origins of the polygons O^k vary from -250 m and 250 m to 750 m and -750 m, respectively (Figure 6b) by an equal step for both of 100 m. We calculated the synthetic data produced by this body, simulating an airborne survey covering an area of 100 km^2 composed of 20 flight lines that are equally spaced from -5000 m to 5000 m and one tie line located at $x = 0$ m, along with the horizontal coordinate y , and with a height of -150 m (Figure 6a). We took out the observation points from a real airborne survey.

We used the same strategy applied to simple model to define z_0 and m_0 . In this case, we chose ranges that do not include the true values of the source's parameters. Therefore, the best solutions are expected to be Γ closer to the true values (red triangle in the map). In Fig. 7, we show the 3 values for the multiple solutions and, also, the red triangle indicates the true pair of z_0 and m_0 and the cyan diamond represents the best pair considering the chosen ranges. As we can see, the lower values of Γ are close to the true pair of z_0 and m_0 .

For this case, the initial guess is a cylinder formed by $L = 8$ prisms, each one with $M = 15$ vertices centered at $(x_0^k, y_0^k) = (-300, 300)$. All prisms that form the initial approximation have the same $r_i = 800, i = 1, \dots, V, \text{ m}$ and depth extent $dz = 650$ m (Figure 6a). We set the weights for the constraints $\tilde{\alpha}_1 = 10^{-4}, \tilde{\alpha}_2 = 10^{-4}, \tilde{\alpha}_5 = 10^{-4}, \tilde{\alpha}_6 = 10^{-7}$, and $\tilde{\alpha}_7 = 10^{-4}$. Again, the third and fourth constraints were not used. Fig. 8a shows the fitting of the inversion of the noise-corrupted total-field anomaly in Fig. 6a. The residuals have a mean and a standard deviation very close to the values of the noise also the histogram is coherent with a Gaussian distribution (Figure 8)a. Due to the lower number of prisms in the interpretation model, the estimated body does not retrieve perfectly the simulated body. However, the volume of the complex model is 12.60 km^3 , while the volume of the estimated source is 12.81 km^3 . Moreover, the estimated depth extent is 6145.12 m, which is very close to 6000 m.

ACKNOWLEDGMENTS**REFERENCES**

- Aster, R. C., Borchers, B., & Thurber, C. H., 2019. *Parameter Estimation and Inverse Problems*, Elsevier, 3rd edn.
- Barbosa, V. C. F., Silva, J. B. C., & Medeiros, W. E., 1997. Gravity inversion of basement relief using approximate equality constraints on depths, *Geophysics*, **62**, 1745–1757.
- Barbosa, V. C. F., Silva, J. B. C., & Medeiros, W. E., 1999b. Stable inversion of gravity anomalies of sedimentary basins with nonsmooth basement reliefs and arbitrary density contrast variations, *GEOPHYSICS*, **64**(3), 754–764.
- Golub, G. H. & Loan, C. F. V., 2013. *Matrix Computations (Johns Hopkins Studies in the Mathematical Sciences)*, Johns Hopkins University Press, 4th edn.
- Horn, R. A. & Johnson, C. R., 1991. *Topics in Matrix Analysis*, Cambridge University Press, 1st edn.
- Marquardt, D. W., 1963. An algorithm for least-squares estimation of nonlinear parameters, *Journal of the society for Industrial and Applied Mathematics*, **11**(2), 431–441.
- Oliveira Jr., V. C. & Barbosa, V. C. F., 2013. 3-D radial gravity gradient inversion, *Geophysical Journal International*, **195**(2), 883–902.
- Oliveira Jr., V. C., Barbosa, V. C. F., & Silva, J. B. C., 2011. Source geometry estimation using the mass excess criterion to constrain 3-D radial inversion of gravity data, *Geophysical Journal International*, **187**(2), 754–772.
- Plouff, D., 1976. Gravity and magnetic fields of polygonal prisms and application to magnetic terrain corrections, *Geophysics*, **41**(4), 727–741.
- Uieda, L., Oliveira Jr., V. C., & Barbosa, V. C. F., 2013. Modeling the earth with fatiando a terra, in *Proceedings of the 12th Python in Science Conference*, pp. 96 – 103.

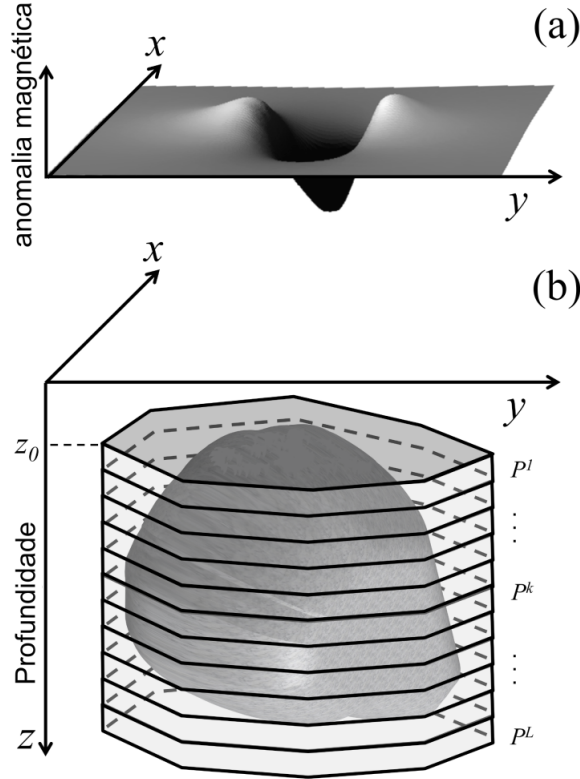


Figure 1. Schematic representation of (a) total-field anomaly (gray surface) produced by (b) a 3-D anomalous source (dark gray volume). The interpretation model in (b) consists of a set of L vertical, juxtaposed 3-D prisms P^k , $k = 1, \dots, L$, (light gray prisms) in the vertical direction of a right-handed coordinate system.

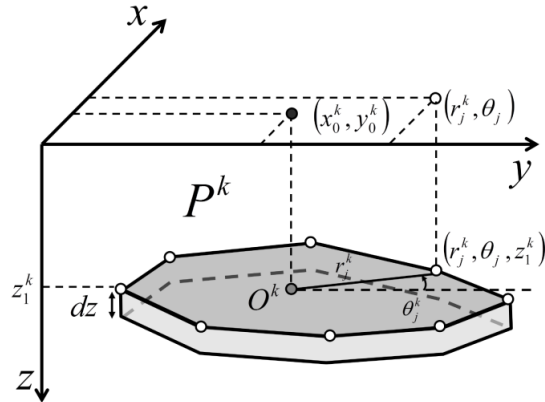


Figure 2. Polygonal cross-section of the k th vertical prism P^k described by V vertices (white dots) with polar coordinates (r_j^k, θ_j^k) , $j = 1, \dots, V$, $k = 1, \dots, L$, referred to an arbitrary origin O^k (grey dot) with horizontal Cartesian coordinates (x_0^k, y_0^k) , $k = 1, \dots, L$.

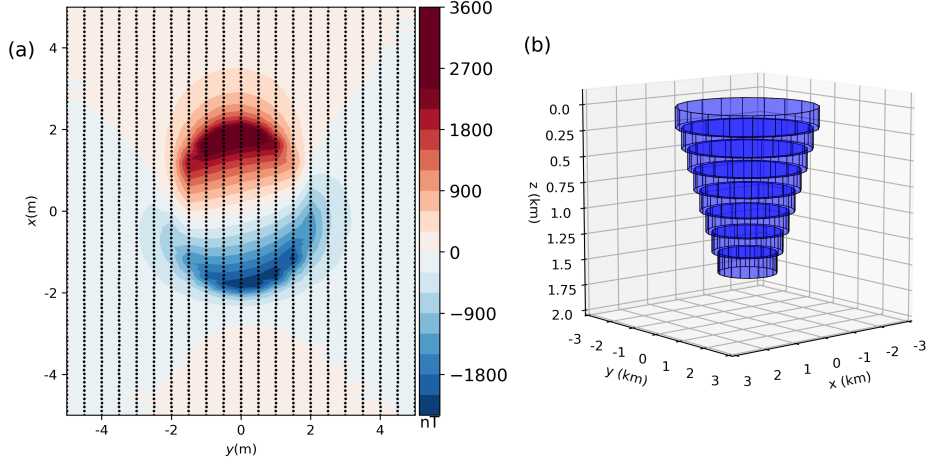


Figure 3. Simple model simulation. (a) noise-corrupted total-field anomaly produced by the simple model (blue prisms) in (b). The black dots represent the observation points simulating an airborne survey.

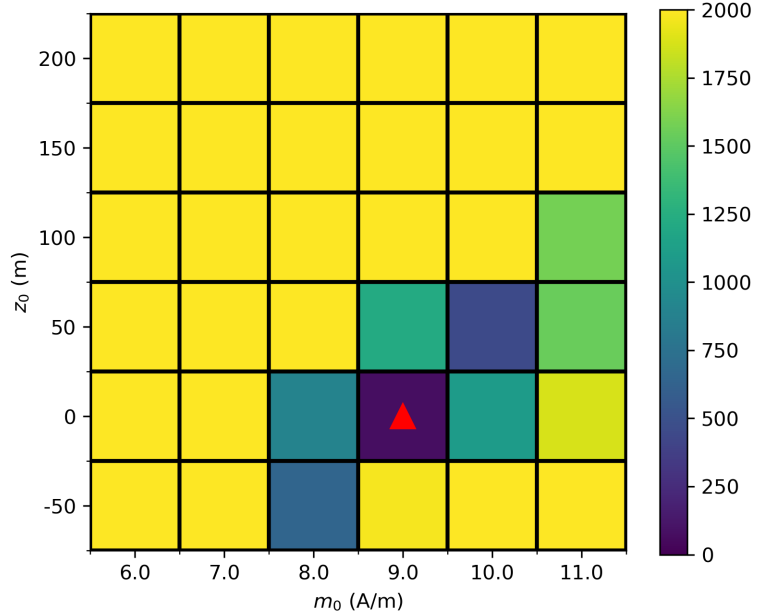


Figure 4. Map of the objective function values due to the inverse solutions for the simple model. The range of m_0 varies from 6 to 11 A/m in a step of 1 A/m and the range of z_0 varies from -50 to 200 m in a step of 50 m. Each square is a value of the goal function (eq. 3) of a solution of the inverse problem for a pair of the total-magnetization intensity and the depth to the top of the source. The red triangle represents the true values for $m_0 = 9 \text{ A/m}$ and $z_0 = 0 \text{ m}$.

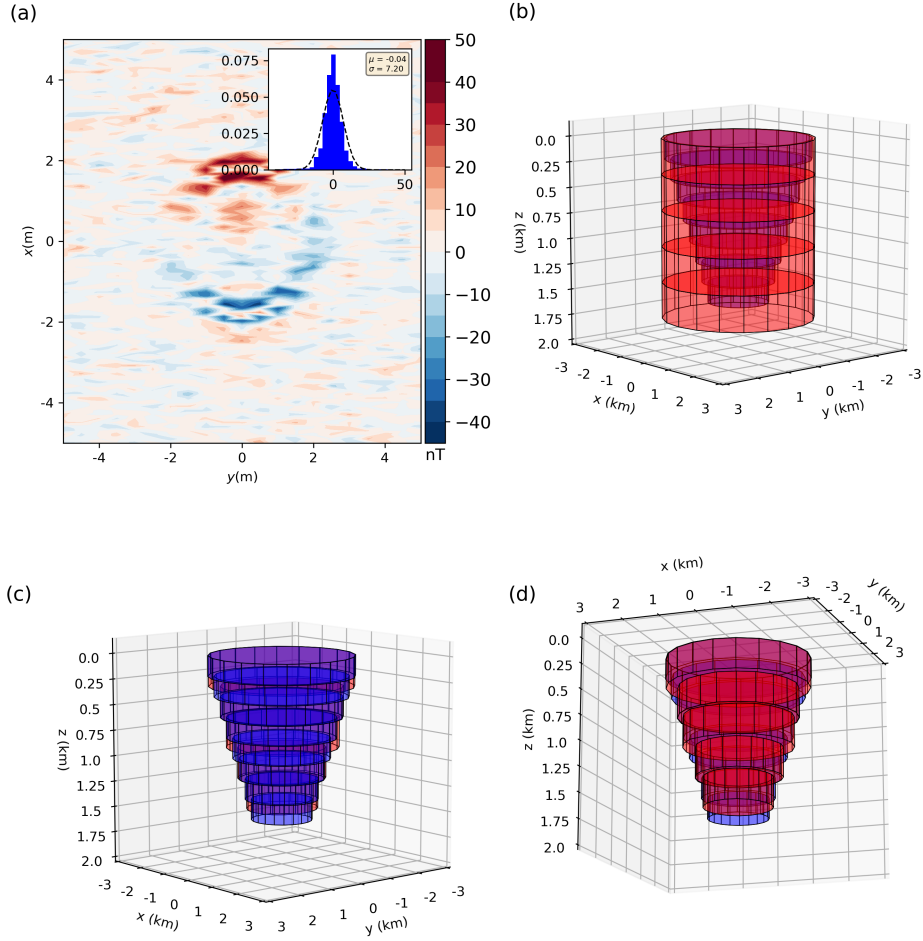


Figure 5. Application to simple model data. (a) residual data given by the difference between the noise-corrupted data (Fig. 3(a)) and the predicted data (not shown) produced by the inverse model (red prisms) in (c) and (d). These inversions were computed using the same cylinder as a initial approximation. The red prisms in (b) represent the input model of the inversion.

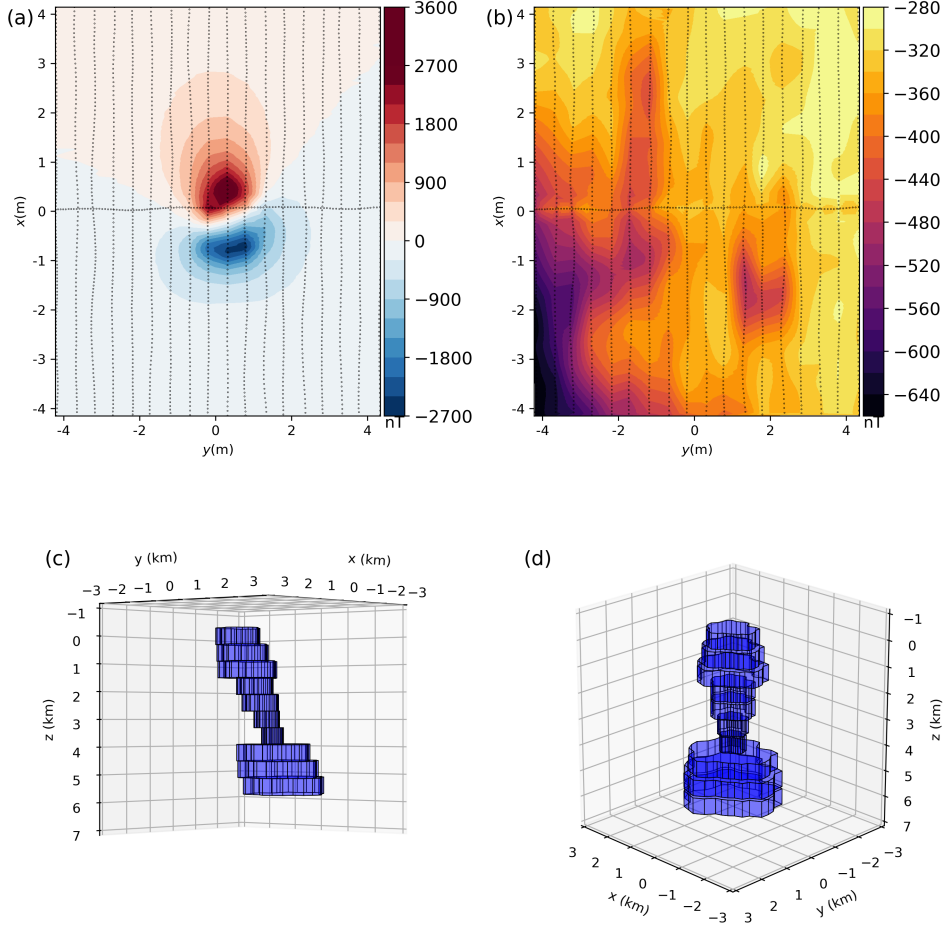


Figure 6. Complex model simulation. (a) noise-corrupted total-field anomaly produced by the complex model (blue prisms) in (c) and (d). The black dots represent the observation points that simulate an airborne survey.

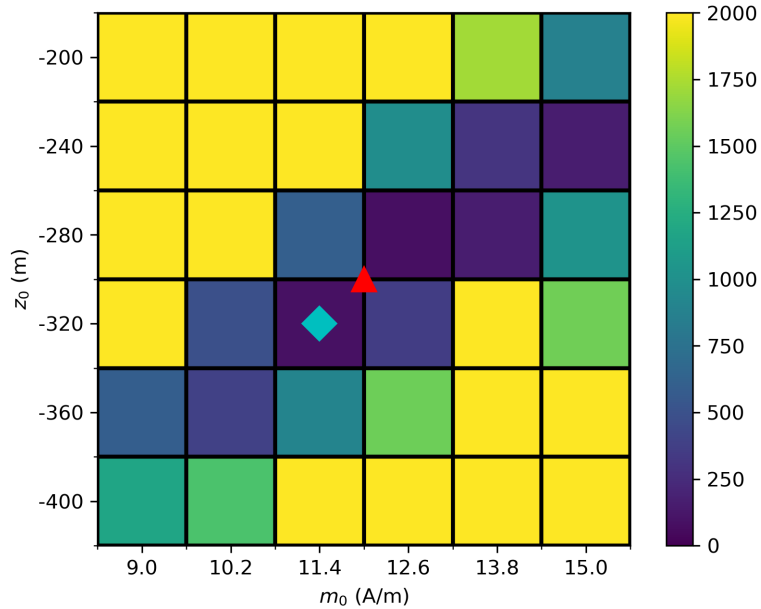


Figure 7. Map of the objective function values due to the inverse solutions for the complex model. The range of m_0 varies from 9 to 15 A/m in a step of 1.2 A/m and the range of z_0 varies from -400 to -200 m in a step of 50 m. Each square is a value of the goal function (eq. 3) of a solution of the inverse problem for a pair of the total-magnetization intensity and the depth to the top of the source. These inversions were computed using the same cylinder as a initial approximation. The red triangle represents the true values for m_0 and z_0 . The cyan diamond represents the solution with the lowest function value.

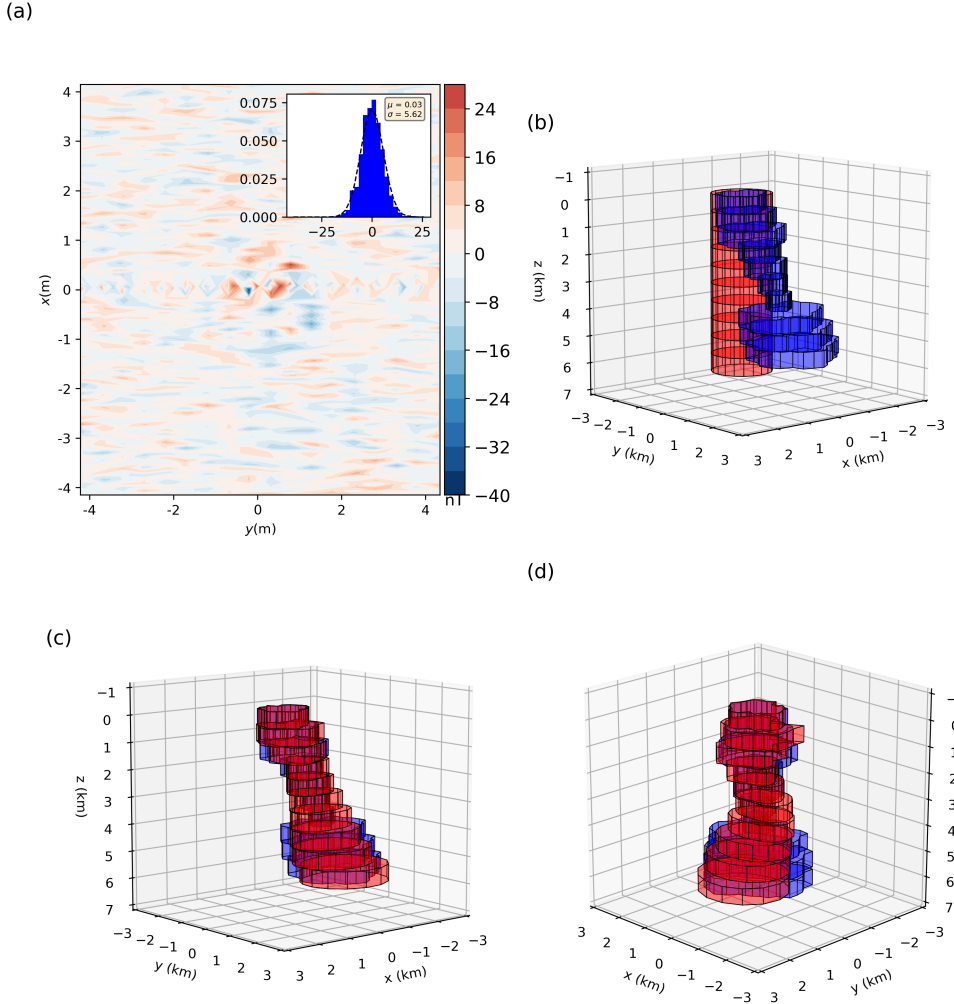


Figure 8. Application to complex model data. (a) residual data given by the difference between the noise-corrupted data (Fig. 6(a)) and the predicted data (not shown) produced by the inverse model (red prisms) in (c) and (d). The red prisms in (b) represent the input model of the inversion.

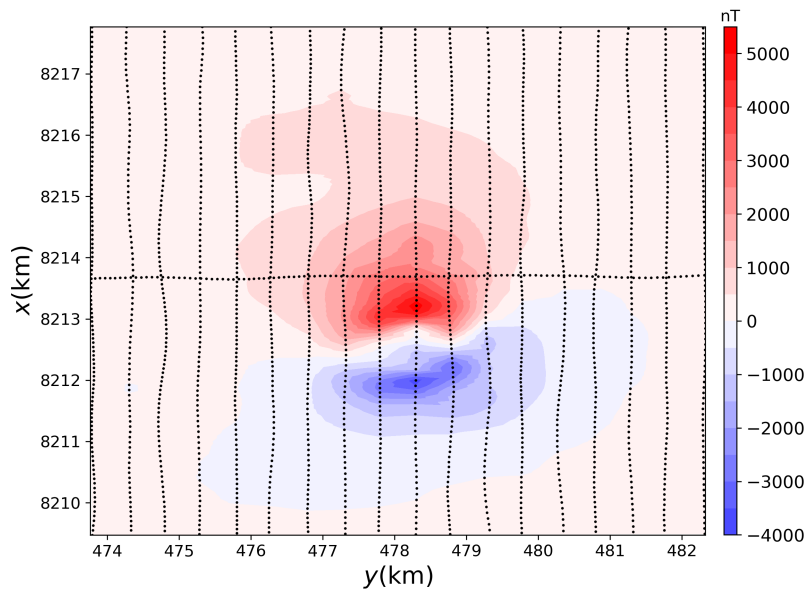


Figure 9. Total-field anomaly of Diorama in GAP. The black dots are the observation points used in this work.

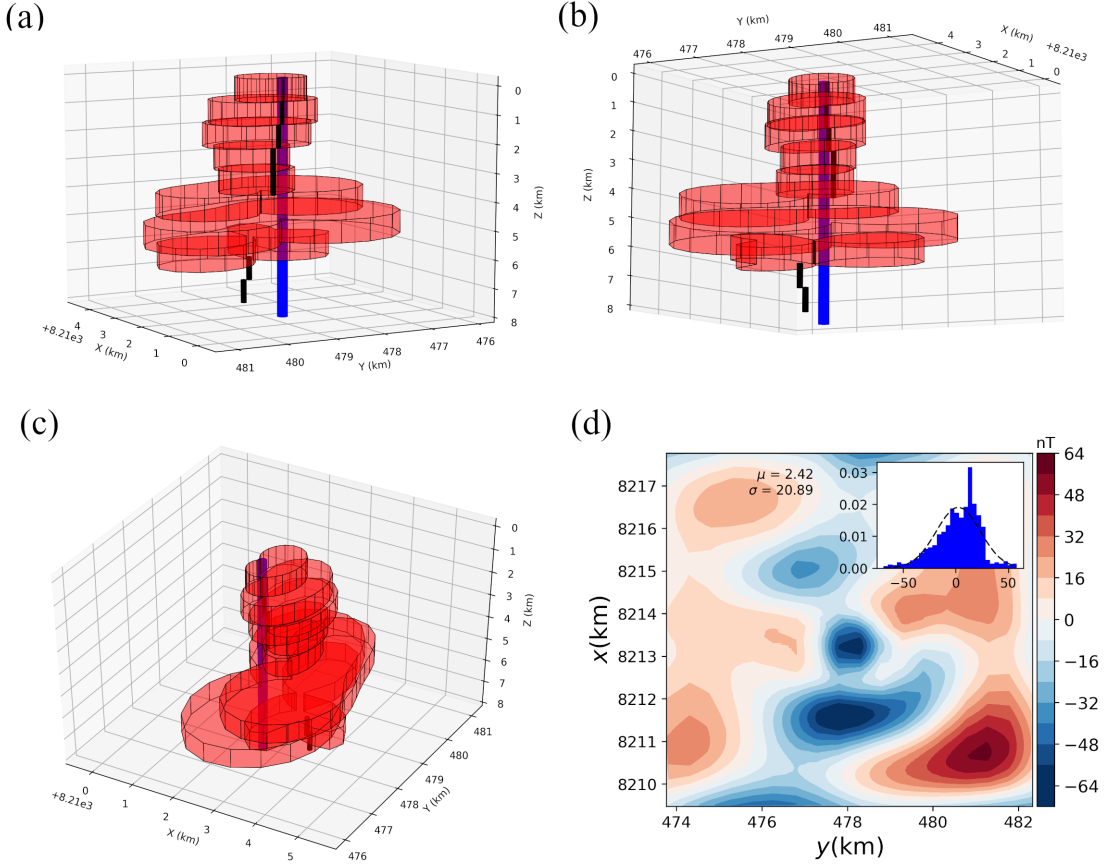


Figure 10. Perspective views of the initial guess (blue cylinder) and the estimated source (red prisms) in (a), (b) and (c). (d) Residuals defined as the difference between the noisy and the predicted (not shown) total-field anomalies and the histogram of the residuals (inset in d) with mean $\mu = 2.42$ nT and standard deviation $\sigma = 20.89$ nT. The dashed line on the inset is the Gaussian curve for the residuals.